Properties of freely decaying and driven turbulence of fusion plasmas using gyrokinetic particle simulation

R. Ganesh*
Institute for Plasma Research, Bhat Village, Gandhinagar - 382 428, India

W. W. LEE, S. ETHIER and J. MANICKAM
Princeton Plasma Physics Laboratory, Princeton, U.S

(Received: 20 November 2009 / Accepted: 6 May 2010)

In a recent work, the effects of nonlinear self-consistent profile relaxation on the ITG turbulence in global delta-f particle simulations were studied [1] using Gyrokinetic Toroidal Code (GTC) [2]. In contrast to several other gyrokinetic turbulence models, GTC shows that the turbulence is insensitive to minute or drastic profile changes and reaches the similar flux levels irrespective of whether or not it is a driven or freely decaying turbulence. In the present work, we address the spectral properties of gyrokinetic turbulence and argue that correct inclusion of parallel velocity space nonlinearity may bring forth certain important late-time features such as Geodesic Acoustic Modes like (GAM) structures.

PACS numbers:
Keywords: gyrokinetics, plasma turbulence, simulation

I. INTRODUCTION

After the discovery of the elongated radial structures associated with the ITG modes (streamers) [3], and the establishment of the importance of the $\mathbf{E}\times\mathbf{B}$ nonlinearity for the spatial trapping and de-trapping of the resonant particles [4, 5], powerful computing capabilities have demonstrated to us the importance of the generation of zonal flows [2], and the energy cascade through mode-coupling processes in toroidal geometry [6]. However, it is not until recently, with the availability of enormous massively parallel computational power, that we have the opportunity to examine the role played by the global zonal flow modes and the nonlinearity associated with the acceleration of the particles in velocity space due to the perturbed field for large tokamaks [7]. It is found that this particular nonlinearity, which has now drawn widespread attention in the fusion community [8], plays an important role in the generation of zonal flows and the ensuing nonlinear ion thermal transport, especially, when we increase the simulation volume. In fact, it is found that this nonlinearity is also responsible for the damping of the zonal flows. Without it, the simulation would fail to converge. Another important question is whether this resulting ion transport is a transient associated with a decay instability or it is indeed some type of steady state phenomena prescribed by the initial profiles. A recent study by taking into account the quasilinear profile relaxation in the simulation has shown that the profile relaxation, which would affect linear stability properties, has negligible effects on the nonlinear ion thermal transport [9]. In this study it is also shown that by removing the wave-particle interaction effects and evolving the late time steady state density and temperature profile as initial value problem leads to a new steady state with lower flux values. In this paper, we shall address the issues of profile relaxation, effect of velocity space nonlinearity on the spectral features of turbulence and its role in formation of Geodesic Acoustic Modes like (GAMs) structures.

II. THE GOVERNING EQUATIONS

The governing equations of the simulation are based on the gyrokinetic Vlasov-Poisson equations [11–13]. In terms of the gyrokinetic units of $\Omega_i(\equiv eB/m_ic)$, $\rho_s(\equiv\sqrt{T_e/T_i}\rho_i)$ for time and space, and $e\phi/T_e$ for the perturbed potential, where ρ_i is the ion gyroradius, and using the Klimontovich-Dupree representation of

$$F_\alpha=\sum_{j=1}^{N}\delta(\mathbf{R}-\mathbf{R}_{\alpha j})\delta(\mu-\mu_{\alpha j})\delta(v_\parallel-v_{\parallel\alpha j}),\quad(1)$$

where F is the phase space distribution in the gyrocenter coordinates of ($\mathbf{R}\equiv\mathbf{x}-\boldsymbol{\rho}$, μ_B, $v_\parallel$), $\mu\equiv v_\perp^2/2$ is the magnetic moment, α denotes species, $\mathbf{x}$ is the usual spatial coordinate, $\boldsymbol{\rho}$ is the gyroradius, the equations of motions are

$$\frac{d\mathbf{R}}{dt}=v_\parallel\hat{\mathbf{b}}+\mathbf{v}_d-\frac{\partial\bar{\phi}}{\partial\mathbf{R}}\times\hat{\mathbf{b}},\quad(2)$$

$$\frac{dv_\parallel}{dt}=-\hat{\mathbf{b}}^*\cdot\left(\frac{v_\perp^2}{2}\frac{\partial}{\partial\mathbf{R}}lnB+\frac{\partial\bar{\phi}}{\partial\mathbf{R}}\right),\quad(3)$$

$$\mu_B\equiv\frac{v_\perp^2}{2B}(1-v_\parallel\hat{\mathbf{b}}\cdot\frac{\partial}{\partial\mathbf{R}}\times\hat{\mathbf{b}})\approx const.,\quad(4)$$

$\hat{\mathbf{b}}^*=\hat{\mathbf{b}}+v_\parallel\hat{\mathbf{b}}\times(\hat{\mathbf{b}}\cdot\frac{\partial}{\partial\mathbf{R}})\hat{\mathbf{b}}$, $\mathbf{v}_d=v_\parallel^2\hat{\mathbf{b}}\times(\hat{\mathbf{b}}\cdot\frac{\partial}{\partial\mathbf{R}})\hat{\mathbf{b}}+\frac{v_\perp^2}{2}\hat{\mathbf{b}}\times\frac{\partial}{\partial\mathbf{R}}lnB$, where $\hat{\mathbf{b}}$ is the unit vector in the direction of

*Electronic address: ganesh@ipr.res.in

the external magnetic field, $\|$ and $\perp$ are the directions parallel and perpendicular to $\hat{\mathbf{b}}$, respectively. The transformation between the gyrocenter coordinates $\mathbf{R}$ and the usual particle coordinates $\mathbf{x}$ associated with a gyroradius $\boldsymbol{\rho}$ yields $\bar{\phi}(\mathbf{R}) = \langle \int \phi(\mathbf{x})\delta(\mathbf{x}-\mathbf{R}-\rho)d\mathbf{x}\rangle_\varphi$, where $\langle\cdots\rangle_\varphi$ is the average over the gyro-angle φ. The corresponding gyrokinetic Poisson's equation [11] becomes

$$\tau[\phi(\mathbf{x}) - \tilde{\phi}(\mathbf{x})] = -\bar{n}_i(\mathbf{x}) + n_e(\mathbf{x}), \tag{5}$$

where $\tilde{\phi}(\mathbf{x}) \equiv < \int \bar{\phi}(\mathbf{R})F_i(\mathbf{R},\mu,v_\|)\delta(\mathbf{R}-\mathbf{x}+\rho)d\mathbf{R}d\mu dv_\| >_\varphi$ is the second average of the gyrophase angle φ on the LHS of the equation, which transforms the $\bar{\phi}(\mathbf{R})$ back to the usual coordinates in $\mathbf{x}$. On the RHS, the densities are defined as

$$\bar{n}_\alpha(\mathbf{x}) = \langle \int F_\alpha(\mathbf{R})\delta(\mathbf{R}-\mathbf{x}+\rho)d\mathbf{R}dv_\|d\mu\rangle_\varphi. \tag{6}$$

Numerically, the transformation between $\mathbf{R}$ and $\mathbf{x}$ can be accomplished through a 4-point average process valid for $k_\perp\rho_i \le 2$ [14]. The δf method, which is based on the scale separation between the background and perturbed quantities [15] and is utilized for the simulations reported in the present paper, is based on Eqs. (2), (3), (4) and

$$\frac{dw}{dt} = -(1-w)\left(\kappa\frac{\partial\bar{\phi}}{\partial\mathbf{R}}\times\hat{\mathbf{b}}\cdot\hat{\mathbf{r}} + \frac{T_e}{T_i}(v_\|\hat{\mathbf{b}}+\mathbf{v}_d)\cdot\frac{\partial\bar{\phi}}{\partial\mathbf{R}}\right), \tag{7}$$

where

$$\kappa = \kappa_n - (3/2 - v^2/2v_{ti}^2)\kappa_{Ti} \tag{8}$$

is the background inhomogeneity with $\kappa_n \equiv 1/L_n$ and $\kappa_{Ti} \equiv 1/L_{Ti}$ representing the spatial gradients in density and temperature, respectively. [Note that the ion acoustic speed c_s is unity in these units.] The perturbed distribution is defined as

$$\delta f_\alpha = \sum_{j=1}^{N} w_j\delta(\mathbf{R}-\mathbf{R}_{\alpha j})\delta(\mu-\mu_{\alpha j})\delta(v_\|-v_{\|\alpha j}),$$

where N is the total number of particle ions in the simulation, $F_\alpha = F_{\alpha 0} + \delta f_\alpha$, $F_{\alpha 0}$ is the background Maxwellian with $\int F_{\alpha 0}d\mathbf{x} = 1$,

$$w \equiv \delta f_\alpha / F_\alpha \tag{9}$$

and $F_\alpha \equiv \delta f_\alpha(w_j = 1)$. For the adiabatic electron model used here, only the evolution of the ion distribution function is followed in time together with a simplified electron density response given by

$$n_e(\mathbf{x}) = 1 + \begin{cases} \phi(\mathbf{x}), & (m,n) \neq (0,0), \\ 0, & (m,n) = (0,0), \end{cases} \tag{10}$$

where (m,n) are the poloidal and toroidal mode numbers, respectively. The approximation used for n_e is adequate for the studies described in the present paper and $\bar{n}_i$ is given by Eq. (6), where $\bar{n}_{i0} = 1$. For the modes with $(m,n) \neq (0,0)$, Eq. (5) can be solved using an iterative scheme [17], whereas, for $(m,n) = (0,0)$, the gyrokinetic Poisson's equation can be simplified for $k_\perp^2\rho_i^2 \ll 1$ as

$$\nabla_\perp^2\phi = -\bar{n}_i + n_e. \tag{11}$$

We should remark here that both Eqs. (5) and (11) are two-dimensional equations perpendicular to the magnetic field.

The parallel nonlinearity is the last term on the right hand side of Eq. (3). This term has not been studied closely in the microturbulence community. However, without this term, the energy conservation cannot be satisfied in the simulation [12, 13]. The only other nonlinearity in the simulation is the last term on the right hand side of Eq. (2), the familiar $\mathbf{E}\times\mathbf{B}$ nonlinearity. It is the key nonlinear term responsible for the nonlinear trapping of the resonant particles [5] and the generation of zonal flows, which, in turn, gives rise to the nonlinear saturation of ITG turbulence and it also regulates the nonlinear state transport by breaking up the streamers. As shown in Ref. [7], the nonlinear generation of zonal flows is also greatly influenced by the velocity space nonlinearity. The terms associated the background inhomogeneity, κ_n and κ_{Ti} in Eq. (8) are usually time independent. Recently, simulations have been carried out by making these terms time dependent to account for the quasilinear changes of the profiles [9], which we will describe.

III. THE SIMULATION CODE AND PARAMETERS

The gyrokinetic toroidal code (GTC) [2, 16] is a particle-in-cell (PIC) code in global geometry based on the gyrokinetic Vlasov-Poisson equations, Eqs. (1)-(11), where the gyrophase averages associated with $\langle\cdots\rangle_\varphi$ were carried out by representing a gyrokinetic particle as a charged ring [14]. An iterative scheme [17] was used to solve the integral part of the gyrokinetic Poisson's equation, Eq. (5), for $(m,n) \neq (0,0)$ modes, and a direct one-dimensional ODE solver in the radial direction was used for $(m,n) = (0,0)$ mode for the zonal flows, both in configuration space. As noted earlier, the electrons are assumed to be adiabatic in the present model, and only the ions are "pushed" in the code. The code uses the magnetic coordinates (ψ,θ,ζ) to describe a tokamak with a circular cross section, where the concentric flux surfaces are represented by $\psi(r)$ in the radial direction, and θ and ζ are the poloidal and toroidal angles, respectively. On the poloidal plane, a 2D mesh with a uniform but unstructured grid in ψ and θ is used with Δ (mesh size) $\approx \rho_i$ (ion gyroradius). The code also uses a global field-aligned mesh [18, 19], taking advantage of the basic property of microturbulence in tokamaks that $k_\| \ll k_\perp$. As such, the resolution in the toroidal direction is closely related to the resolution in the poloidal direction resulting in a reduction in number for the toroidal grid [18, 20, 21]. A slight shift of the field lines is then

needed in order to match the mesh in the code [16, 18]. A more complete form of Poisson's equation in the presence of adiabatic electrons can be written as

$$\tau[\phi(\mathbf{x}) - \tilde{\phi}(\mathbf{x})] - [\phi(\mathbf{x}) - \langle\phi(\mathbf{x})\rangle] = -\delta\bar{n}_i(\mathbf{x}), \qquad (12)$$

where $\langle\cdots\rangle$ denotes flux surface average and δn_i is the perturbed ion response. When long wavelength large amplitude waves co-exist with short wavelength small amplitude waves in a system such as ours, more accurate treatments are needed to solve this equation, which has been implemented in our latest Gyrokinetic Tokamak Simulation (GTS) code, which can use the experimental measurements as input [22].

The Cyclone-based-parameters [23] have been used for the simulation with 64 toroidal grid points for $a/\rho_i = 125$ on each poloidal plane, where a is the minor radius of the tokamak. Thus, the shortest wavelength modes that can be resolved in the code are of the order of $k_\perp\rho_i \approx 2$. The other parameters are: $n_0 = 40 - 80$ (number of particles per cell), $R/L_T = 6.9$, $R/a = 2.79$, $L_n/L_{Ti} = 3.13$, $\Omega_i\Delta t = 7.6$ and $T_e/T_i = 1$. All these runs have been conducted by taking into account of all the physics described in Eqs. (2) - (3), including the nonlinearly generated zonal flows and the velocity space nonlinearity. Typically two kinds of profiles are used: one is an exponential profile of the inhomogeneity is given by $(1/L)e^{-[(r-r_c)/r_w]^6}$, where L represents either the temperature scale length L_{Ti} or the density scale length L_n with $r_c/a = 0.5$ and $r_w/a = 0.35$, while the other is a cosh-profile whose inhomogeneity is given by $(1/L)cosh-[(r-r_c)/r_w]^2$ Note that while the exponential profile is broad at the center and varies slowly, the cosh-profile varies much more rapidly so that profile-effects, if any, could come into play.

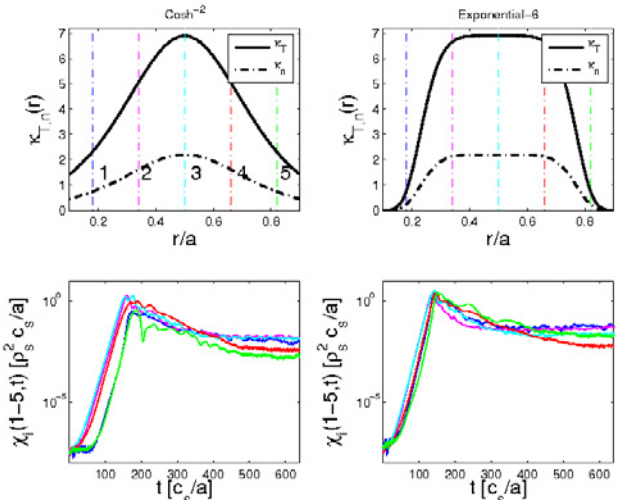

FIG. 1: Two different density/temperature profiles (Top Row) are used for driving the ITG modes. Note that in the "Cosh-profile", profile variation effects, if any, would appear whereas in the "Exp-profile", the core is nearly flat. Five different locations radial locations (1-5) where various quantities measured will be displayed. (Bottom Row) Fluxes at 5 locations shown as the function of time for upto 700 c_s/a times.

IV. PROFILE RELAXATION AND ITG TURBULENCE

To understand the issues of profile relaxation in gyrokinetic PIC simulations using the δf method, we have performed simulations using the exponential/cosh profiles as initial conditions for the background inhomogeneity and we have also kept track of the quasilinear modifications of the profiles during the course of the simulation, i.e.,

$$\kappa_{Ti} = -\frac{1}{T_{0i}}\frac{d(T_{0i} + \delta T_{0i})}{d\epsilon x}$$

and

$$\kappa_n = -\frac{1}{n_{0i}}\frac{d(n_{0i} + \delta n_{0i})}{d\epsilon x},$$

where δT_{0i} and δn_{0i} are the flux surface averaged evolution. However, there is no back reaction of the profile changes to the simulated turbulence. In Fig.1 (top row), the drives for both profiles are plotted and the corresponding fluxes at 5 different locations. Next, simulations that taking into account the profile modifications of the zeroth-order profiles, given above, have then been carried out. The comparisons of these two sets of results should give us some indication of the effects of profile relaxations on the simulations of ITG turbulence. As shown in. Fig. 2, where the time evolution of the profiles are plotted, the profile for the temperature gradient has been modified by more than $\pm 15\%$ at the end of the simulation, whereas the density gradient modification is small and mainly due to noise, as expected. Surprisingly, as shown in Fig.3, no noticeable changes of the resulting thermal fluxes have been detected between the two cases. These results raise the question concerning whether ITG modes are really "stiff" and whether we have reached some kind of steady state. Details of the simulations can be found in Ref. [9].

Further it is found that the system attains a quasi-steady state in the absence of source or sink. It is expected that this is due to the nonlinear wave-particle interaction. This idea can be tested in the following manner. In GTC evolution where profile changes are included, we start with $R/L_T \simeq 6.9$ as shown in Fig.4 for Cosh-profile. Initial profile is in continuous magenta color. The final state is shown in red. Clearly the turbulence has evolved at the cost of free energy in the gradients resulting in waves and interacting particles. The corresponding fluxes during the evolution is shown on the right panel. Note that the flux at late times, has arrived at a quasi-steady state. The background gradients have stopped evolving; this arrest comes about due to wave-particle interaction. If we now restart the simulations, after removing the wave-particle physics (by resetting

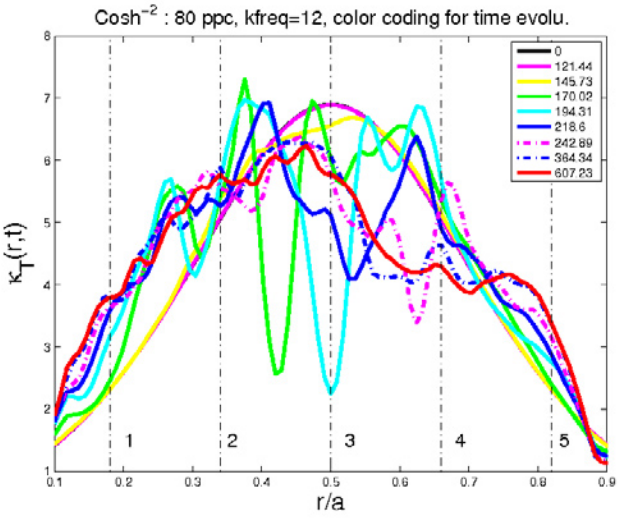

FIG. 2: Freely evolving turbulence : background profile evolution of κ_T profiles is shown for Cosh-profile. Density also evolves, however, the relative changes are weaker compared to temperature gradient evolution. Note that as time evolve, in the linear stage, substantial changes in κ_T are observed with less changes towards late times showing quasi-steady state. Similar evolution is seen for Exp-profile.

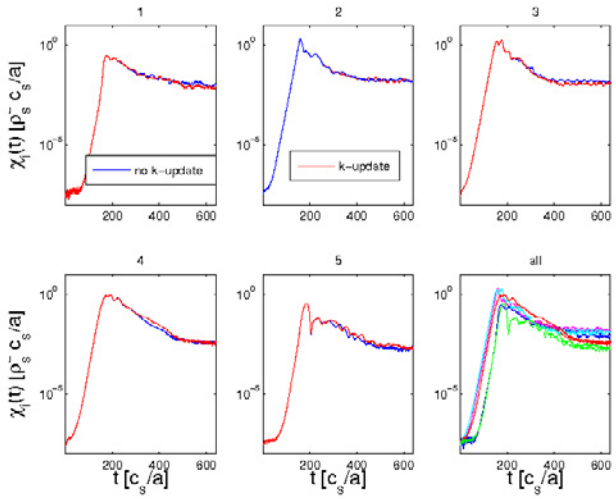

FIG. 3: Comparison of fluxes at five different locations indicated in Fig.1: Profile changes shown in Fig.2 does not seem to affect the resultant flux, thus casting doubts on issues of "stiffness" in ITG turbulence.

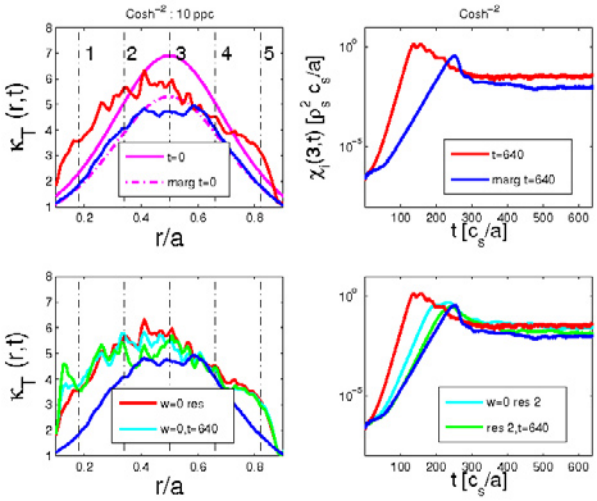

FIG. 4: March towards marginality: For Cosh-profile, in order to determine the role of wave-particle interaction, after quasi-steady state is reached, the particle weights w are reset to zero and the system is restarted from the new steady state. This successive relaxation evolves every time to a new quasi-steady state with relative low flux values.

the particle weights w to zero) and with the final background profiles (see Fig.4 lower left panel), we see that the new linear stage, followed by a new steady state with a new background profile is seen. We have repeated this process to show that the profiles alter the linear characteristics and wave-particle interaction leads to a new quasi-steady state. A similar physics is seen for Exp-profile shown in Fig.5. Note that in the restart runs, the zonal flow potential has not been included. Hence several restarts may systematically bring down the final R/L_T values. However, if one includes the zonal potential, then this process of instability followed by background profile modification, generation of wave-particle interaction and saturation should stop at a finite value of R/L_T.

V. $v_{||}$ NONLINEARITY AND FORMATION OF GAM-LIKE $m = 1$ STATE

Standard Geodesic Acoustic Modes [10] were first predicted in 1968. These are electrostatic potential perturbations with mode number ($m = 0$, $n = 0$) and density perturbations with ($m = 1$, $n = 0$). Generation, sustenance and damping of standard GAMs is subject of intense research [24, 25] as they are associated with zonal flows which regulate transport due to low frequency drift wave turbulence. Standard GAMs have real frequency $\simeq c_s/R$ where c_s is the ion sound speed and R is the major radius. They are either oscillatory or damped modes: damping rate is typically small for large q values and reduces with collisionality. Thus it can be expected that in a collisionless plasma, standard GAM oscillations would survive over ion-ion collision time and should be observable in late-time states of collisionless gyrokinetic simulations. It is also known that several GAM-like branches of standard GAM mode exists as has been reported recently in [24, 25] as eigenmode problem. Standard GAMs have

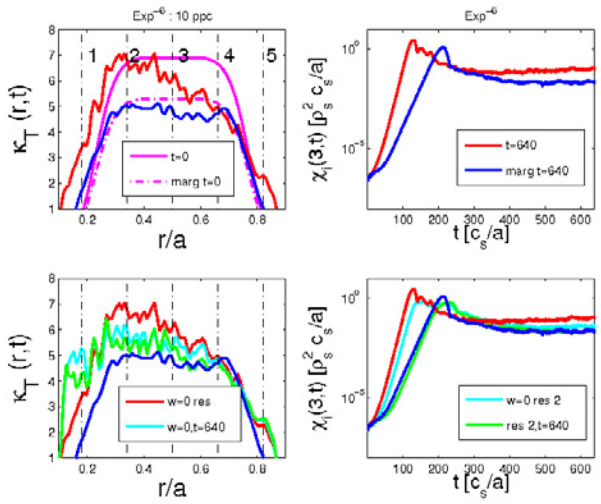

FIG. 5: Same as Fig.4 but for Exp-profile

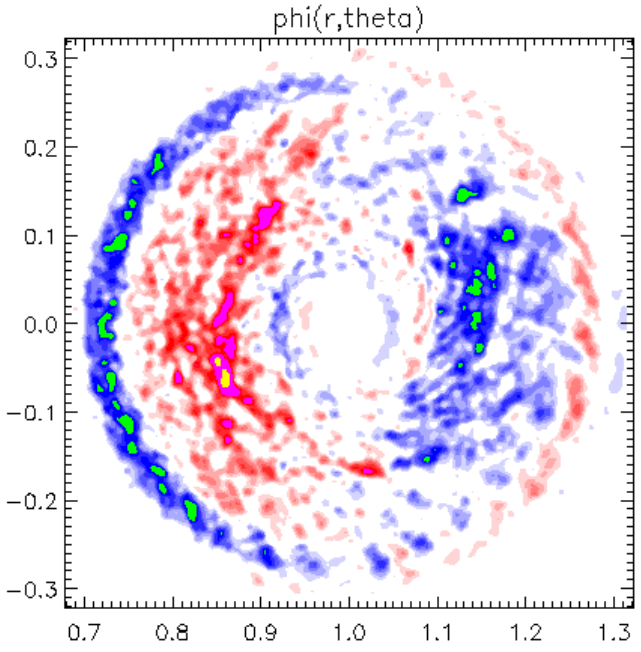

FIG. 6: Mode structure of GAM-like $m = 1$ potential perturbation is shown when PNL=1. In our simulations, seed for this global, low $k_r\rho_i$ mode forms just after the nonlinear phase and sustains without damping throughout the late-time evolution.

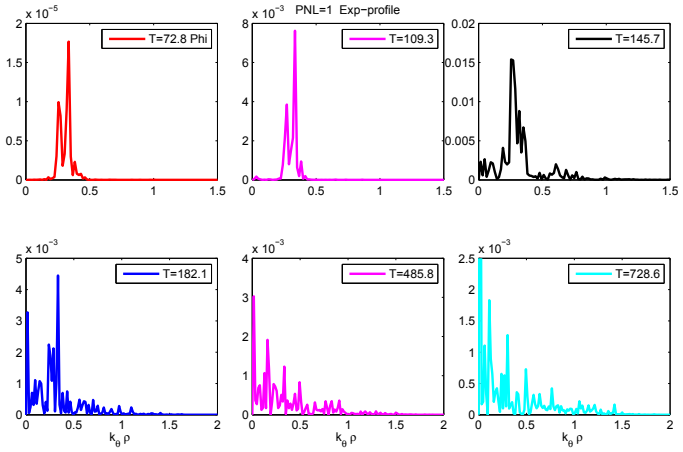

FIG. 7: Evolution of Potential Fluctuation Spectrum with parallel velocity nonlinearity (PNL). As time progresses, the power in the fluctuations are seen to move towards larger scales demonstrating at late times large scale fluctuations are dominant

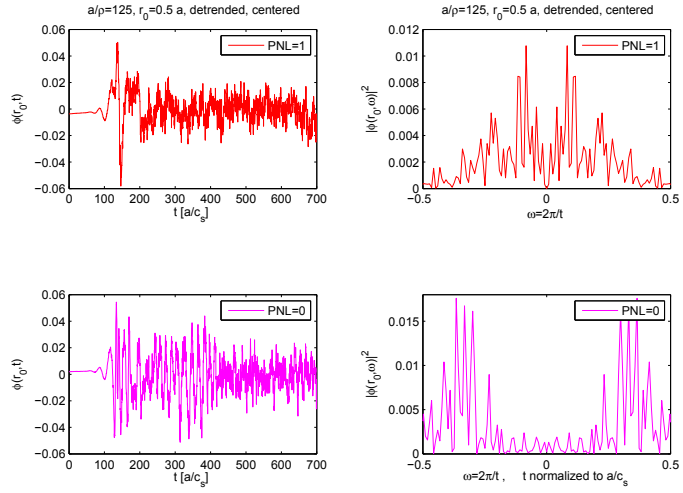

FIG. 8: Effect of parallel velocity nonlinearity (PNL) on the frequency spectrum of large scale GAM-like potential structure is shown. Top row shows electric potential time series and its frequency spectrum measured at $r = 0.5a$ with parallel nonlinearity on (PNL=1). On the bottom row is the case with PNL=0. Frequency obtained for the case with PNL=1 appears to match with theoretical estimates.

radial structure akin to zonal flows $k_r\rho_i \simeq 1$ where k_r is the radial mode number.

Here, undamped, global, GAM-like structures are reported with GTC simulations, which appear as the late-time states of gyrokinetic simulations. These GAM-like potential perturbations have $m = 1$ and $n = 0$ and are global with $k_r\rho_i \ll 1$, as shown in Fig.6. It is observed that $v_{||}$-nonlinearity is fundamental to the development of this global GAM-like structure. Inclusion of this $v_{||}$-nonlinearity not only produces a late time state as that of an GAM-like structure but also results in a frequency spectrum for our $q-$values close to the frequency of standard GAM modes. Note that the GTC simulations which include $v_{||}$ nonlinearity always produce global zonal flow structures with $k_r\rho_i \ll 1$.

It is further demonstrated that the global GAM-like structure is a result of an inverse cascade in poloidal mode number $k_\theta\rho_i$. In Fig.7 we analyze the potential fluctuations from linear stage in time to the fully nonlinear and

finally at saturated stage. At the linear state, as can be expected, the fluctuation peaks at $k_\theta \rho_i \simeq 0.4$ consistent with the linear stability models. As time evolves, due to quasi-two dimensional nature of the Tokamak geometry $k_{||} \ll k_\perp$, an inverse cascade in power spectrum $|\phi|^2$ is seen clearly. For example, as time evolves, the spectral peaks at smaller and smaller values of $k_\theta \rho_i$ eventual reaching values where $m \simeq 1$. Thus leading to a global $m = 1$ GAM-like structure in the presence of $v_{||}$ nonlinearity. In Fig.8, we have obtained the frequency of fluctuations at one point in (r, θ, ϕ) in this late time state. Spectrum with and without $v_{||}$ nonlinearity are clearly seen to be different. Following Gao et al [25], we consider for our values of q, the expression $\omega_{GAM} \simeq \pm 0.2(1 + 0.4\tau)(\sqrt{2}v_{ti}/qR)\sqrt{(}1 - (1.2/q)^2)$ for $\xi \equiv qR\omega/\sqrt{2}v_{ti} \ll 1$ and $q > 1.2$, ω_{GAM} turns out to be of the order $\omega_{GAM} \simeq 0.05 c_s/R$ for $\xi = 0.14$ and $R/a = 2.79, \tau = 1$. which is about the value obtained including $v_{||}$ nonlinearity.

VI. CONCLUSION

The effects of nonlinear self-consistent profile relaxation on the ITG turbulence in global delta-f particle simulations using Gyrokinetic Toroidal Code (GTC) has been reported. GTC shows that the turbulence is insensitive to minute or drastic profile changes and reaches the similar flux levels irrespective of whether or not it is a driven or freely decaying turbulence. Spatial and temporal spectral properties of gyrokinetic turbulence appear to indicate that correct inclusion of parallel velocity space nonlinearity may bring forth certain important late-time features such as Geodesic Acoustic Modes (GAM).

[1] W. W. Lee, S. Ethier, R. Ganesh, R. Kolesnikov and W. X. Wang, AIP Conf. Proc. **1069**, 144 (2008).
[2] Z. Lin, T. S. Hahm, W. W. Lee, W. M. Tang and R. White, *Science*, **281**, 1835 (1998).
[3] S. E. Parker, W. W. Lee, and R. A. Santoro, Phys. Rev. Lett. **71**, 2042(1993).
[4] W. W. Lee and W. M. Tang, Phys. Fluids **31**, 612 (1988).
[5] S. E. Parker et al., Phys. Plasmas **1**, (5): 1461 (1994).
[6] W. X. Wang et al., Phys. Plasmas **14**, 072306 (2007).
[7] W. W. Lee, S. Ethier, R. Kolesnikov, W. X. Wang, and W. M. Tang, "Nonlinear Turbulent Transport in Magnetic Fusion Plasmas," PPPL-4275, submitted to Computational Science and Discovery (2008).
[8] L. Villard et al., Plasma Phys. Contr. Fusion **46**, B51 (2004).
[9] R. Ganesh, W. W. Lee, R. Kolesnikov, S. Ethier, and J. Manickam, "Effects on Profile Relaxation on Ion Temperature Gradient Drift Instabilities," invited talk, 20th International Conference on Numerical Simulations of Plasmas, Austin, TX (2007)
[10] N. Winsor, J. L. Johnson, J. J. Dawson, Phys. Fluids **11**, 2248 (1968).
[11] W. W. Lee, Phys. Fluids **26**, 556 (1983).
[12] D. E. Dubin, J. A. Krommes, C. Oberman and W. W. Lee, Phys. Fluids **26**, 3524 (1983).
[13] T. S. Hahm, Phys. Fluid **31**, 2670 (1988).
[14] W. W. Lee, J. Comp. Phys. **72**, 243 (1987).
[15] S. E. Parker, and W. W. Lee, Phys. Fluids B **5**, 77 (1993).
[16] S. Ethier, W. M. Tang, and Z. Lin, J. Phys.: Conf. Series **16**, 1 (2005).
[17] Z. Lin and W. W. Lee, Phys. Rev. E **52**, 5646 (1995).
[18] Z. Lin, S. Ethier, T. S. Hahm, W M. Tang, Phys. Rev. Lett. **88**, 195004 (2002).
[19] A. M. Dimits, Phys. Rev. E **48**, 4070 (1993).
[20] B.Scott, Phys. Plasmas. **5**, 2334 (1998).
[21] W. X. Wang et al., Phys. Plasmas **13**, 092505 (2006).
[22] W. X. Wang et al., Phys. Plasmas **14**, 072306 (2007).
[23] A. M. Dimits, G. Batemen, M. A. Beer et al., Phys. Plasmas **7**, 969 (2000).
[24] Z. Gao et al, Phys. Plasmas **13** 100702 (2006)
[25] Z. Gao et al, Phys. Plasmas **15** 072511 (2008)